Journal of Beijing Institute of Technology, 2020, Vol. 29, No. 4

Resonance Suppression Strategy for Humanoid Robot Arm

Weiling Zhang, Qinjun Du✉, Zhengyang Zhao, Chuanming Song, Wei Ding and Yonggang Luo

(School of Electrical and Electronic Engineering, Shandong University of Technology, Zibo 255049, Shandong, China)

Abstract: To address the problem of resonance in the control of a robot arm, a resonance suppression strategy is proposed for a single-joint humanoid robot arm based on the proportional-resonant (PR) controller. First, an arm joint model of the humanoid robot is established. Then the influence of resonance frequency on the performance of the control system with the robot arm is analyzed. The voltage fluctuation of the drive motor caused by the changes in arm motion is recognized as the disturbance of the current loop. The PR controller has the characteristic of disturbance rejection at a specific frequency. The output fluctuation of the driving system caused by the change of arm motion state at the resonance frequency is suppressed. Therefore the output current of the inverter will not be affected by the vibration of the arm at the resonance frequency. Finally, the control system is verified by MATLAB/Simulink simulation. The simulation results demonstrate that the control strategy for the humanoid robot arm based on the PR controller can suppress the resonance of the arm effectively, improving the dynamic performance and system stability.

Key words: humanoid robot arm; resonance; proportional-resonant (PR) controller; disturbance rejection

CLC number: TM301.2 **Document code:** A **Article ID:** 1004-0579(2020)04-0456-10

Humanoid robots have human appearance characteristics, as well as the functions corresponding with their appearance features. Humanoid robots are widely applied to dangerous operations, medical treatment, service business, and so on. It can replace human to handle many operations in various tasks without changing the work environment, so it has a broad application prospect. The performance of humanoid robot arm will affect the completion of a task. Harmonic reducer is often used in humanoid robot arm to connect motor with arm link. The inherent flexibility in harmonic driver produces resonance frequencies. When control frequency equals to the resonance frequency of arm, the resonance phenomenon will occur. The resonance not only harms the structure of the joint and affects its service life but also leads to controlled quantities to oscillate in the robot arm control system. The operation performance of the humanoid robot arm and the stability of the system are seriously affected. Therefore, the resonance suppression strategy is indispensable in motion control of humanoid robots.

A number of studies on the vibration of robotic arms have been performed at present[1-3]. In the motion control field, many resonance suppression control methods such as notch filter, resonance ratio control and self resonance cancella-

Received 2020-02-24
Supported by the National Key Technology Research and Development Program of China (2018YFC1707104); National Natural Science Foundation of China (62076152); Natural Science Foundation of Shandong Province (ZR2017MF045); Beijing Advanced Innovation Center for Intelligent Robots and Systems
✉ Author for correspondence
E-mail: duqinjun@sdut.edu.cn
DOI: 10.15918/j.jbit1004-0579.20020

tion and so on are proposed. Yang et al.[4] used a notch filter to attenuate the amplitude of specified frequency without affecting other frequencies. The resonance of industrial robots is effectively suppressed. Ref. [5] used the zero phase error notch filters in order to suppress the vibration phenomenon which is generated by the resonant frequency and the nonlinear interference force from the other joints of robot. It realizes the fast accurate robot motion control without vibration phenomenon and overshoot. However, improper design parameters of notch filter will lead to phase angle advance or lag of other frequency signal near the resonant frequency. Besides, the resonance of two different frequencies will be inducted into the system while the mechanical resonance is suppressed by the notch filter. Hence the mechanical resonance cannot be eliminated completely. An adaptive notch filter has the advantage over a notch filter because an adaptive one can automatically adjust the notch frequency to the resonant frequency[6-7]. However, the parameters of adaptive notch filter are difficult to meet the requirements when high frequency resonance occurs. The deviation between the resonance frequency and the resonant peak frequency will lead to the failure of the proposed method. Ref. [8] adopted slow resonance ratio control for vibration suppression and disturbance rejection in the torsional system. The phase margin of the system decreases when the nominal inertia of the motor is greater than the actual inertia of the motor. And large deviation will cause system instability. It was possible to design a feedback controller which not only broadens the bandwidth but also improves the robustness against the resonance mode parameters using the self resonance cancellation (SRC) method[9]. The primary resonance mode is cancelled by using SRC and the second resonance can be reduced by adjusting the mechanical parameter. However, because SRC does not take modeling errors into consideration, it is difficult to be applied to a humanoid robot which changes moment of inertia, centrifugal force, coriolis force, gravity, frictional force according to the postual changes. Moreover, SRC has a problem that a steady-state error arises due to load side disturbance torque. A robust control method for two inertia systems was proposed based on SRC and the self resonance cancellation disturbance observer (SRCDOB)[10]. The proposed robust resonance suppression control method is applied to a humanoid robot control system and experimental results demonstrate the effectiveness of the proposed robust. Nevertheless, the control algorithm has many setting parameters and the design procedure is complicated. A lot of debugging and trial and error is required in the actual simulation process. From above analysis, the previous methods fail to solve the resonance of humanoid robot arm caused by joints flexibility.

In order to suppress the resonance of the robot arm and achieve a good control effect, this paper proposes a resonance control strategy for humanoid robot arm based on proportional-resonant (PR) controller[11-13]. The gain of the PR controller at the resonance frequency is infinite, which can guarantee the zero-tracking-error for sinusoidal reference. Moreover, there is no attenuation outside that frequency. As a result, it can be used as a notch filter so that it suppresses the vibration at a specific frequency. The PR controller has the characteristic of disturbance rejection at the specific frequency without affecting the performance at other frequencies. Therefore, the control frequency is not equal to the arm resonant frequency so that the self-excited vibration will not be excited. The proposed strategy improves performance and ensures the stability of the system. The scheme can suppress the resonance of the humanoid robot arm and has a good control effect.

1 Analysis of Resonance for Humanoid Robot Arm

1.1 Arm joint modeling

As to humanoid robots, a high load-to-weight ratio is a key requirement. The compact

high-gear reduction, such as the harmonic reducer is frequently used in the driving system for the sake of high load-to-weight performance. The flexibility of the robot arm joint increases due to the harmonic driver. Also, joint flexibility plays a role of protection to the robot arm and extends its service life.

A simplified model for the single-joint humanoid robot arm is established based on the model of a flexible joint robot proposed by Spong[14], as shown in Fig. 1. The joint flexibility is modeled as a linear spring with stiffness, where K is the joint stiffness and N is the gear ratio.

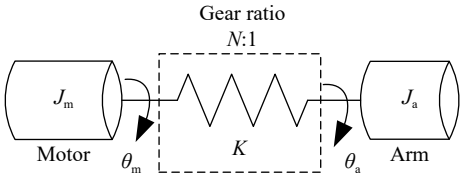

Fig. 1 Simplified model for humanoid robot arm

The mathematical model of humanoid robot arm joint is established based on the momentum conservation of the system and the Lagrange equation[15]. Its dynamical equation is

$$\begin{bmatrix} J_m & 0 \\ 0 & J_a \end{bmatrix} \begin{bmatrix} \ddot{\theta}_m \\ \ddot{\theta}_a \end{bmatrix} + \begin{bmatrix} 0 \\ V \end{bmatrix} + \begin{bmatrix} 0 \\ G \end{bmatrix} + \begin{bmatrix} F_m \\ F_a \end{bmatrix} = \begin{bmatrix} T - \tau \\ \tau \end{bmatrix} \quad (1)$$

where J_m is the motor inertia; J_a is the arm inertia; θ_m is the angle of the motor; θ_a is the angle of the arm; V is a vector containing the Coriolis force and centrifugal force; G is the gravity torque; F_m is the friction torque of motor; F_a is the friction torque of robot arm joint; T is motor output torque.

The dynamical Eq. (1) is decomposed

$$\begin{cases} J_m\ddot{\theta}_m + F_m = T - \tau \\ J_a\ddot{\theta}_a + V + G + F_a = \tau \end{cases} \quad (2)$$

The first formula in Eq. (2) is the dynamical equation of drive motor, and the second formula is the dynamical equation of the humanoid robot. The joint torque τ from harmonic driver to joint generated by joint flexibility is given by

$$\tau = K(\theta_m - \theta_a) \quad (3)$$

Here, a brushless DC motor is used as the driving motor for the humanoid robot arm joint, and the voltage equations can be described as

$$u_x = Ri_x + L\frac{\mathrm{d}i_x}{\mathrm{d}t} + e_x,\ x = a, b, c \quad (4)$$

where u_x represents the terminal phase voltage concerning power ground; i_x represents the rectangular-shaped phase current; e_x represents the trapezoidal-shaped back-EMF. The constants R and L represents the resistance and equivalent inductance of the phase windings, respectively.

The motor torque T_e is

$$T_e = \frac{e_a i_a + e_b i_b + e_c i_c}{\Omega} \quad (5)$$

where the motor speed Ω is given by

$$\Omega = \frac{\mathrm{d}\theta_m}{\mathrm{d}t} \quad (6)$$

1.2 Resonance mechanism analysis

From above analysis, the mathematical model of humanoid robot arm joint contains nonlinear terms. Here the nonlinear terms of the robot arm are ignored for the sake of analysis; the following equation can be derived from Eq. (2).

$$\begin{cases} J_a\ddot{\theta}_a = K(\theta_m - \theta_a) \\ J_m\ddot{\theta}_m + K(\theta_m - \theta_a) = T \end{cases} \quad (7)$$

The block diagram of the humanoid robot arm joint is shown in Fig. 2.

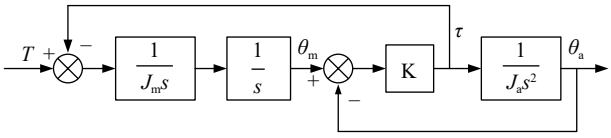

Fig. 2 Block diagram of humanoid robot arm joint

The closed-loop transfer functions from the motor torque to the motor and arm angle, respectively, for the control structure, demonstrated in Fig. 2, are given as

$$\frac{\theta_m}{T} = \frac{1}{J_m s^2} \frac{J_a s^2 + K}{J_a s^2 + K(1 + J_a/J_m)} \quad (8)$$

$$\frac{\theta_a}{T} = \frac{1}{J_m s^2} \frac{K}{J_a s^2 + K(1 + J_a/J_m)} \quad (9)$$

The transfer function is shown in Eq. (8) contains a pair of imaginary conjugate poles and

a pair of imaginary conjugate zeros. The imaginary conjugate poles in Eq. (9) are the same as the ones in Eq. (8). The introduced imaginary conjugate poles and zeros will reduce the performance of humanoid robot arm motion system. It could have a strong influence on the control quality of the drive system and the practical operation effect. Here, the conjugate zeros introduce the anti-resonance frequency (ARF), and the conjugate poles introduce the natural torsional frequency (NTF) of the system, namely, the resonance frequency. The resonance frequency of the motor portion and the anti-resonance frequency of the arm portion are defined as follows

$$\begin{cases}\omega_{\mathrm{NTF}}=\sqrt{\dfrac{K}{J_{\mathrm{a}}}(1+J_{\mathrm{a}}/J_{\mathrm{m}})}\\ \omega_{\mathrm{ARF}}=\sqrt{K/J_{\mathrm{a}}}\end{cases}\tag{10}$$

Fig. 3 shows the block diagram of the humanoid robot system. In Fig. 3, k_1 and T_1 represent the proportionality coefficient and the time constant of the speed PI controller, respectively. T_{s} is the time constant of the inertia link.

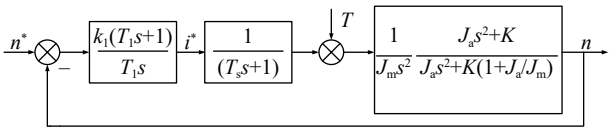

Fig. 3 Block diagram of the closed-loop system

Bode plot of the open-loop and closed-loop systems can be obtained in Fig. 4. It is observed that there exist a resonance frequency and an anti-resonance frequency in the humanoid robot control system. As to amplitude characteristics, the open-loop gain at resonance frequency increases sharply, and the case at the anti-resonance frequency is the opposite. The closed-loop pole is farther away from the imaginary axis than the open-loop pole, that is, the closed-loop resonance frequency is larger than the open-loop resonance frequency. Therefore, the amplitude characteristics vary dramatically at the frequency equal to NTF and ARF as a consequence of joint flexibility. It is not beneficial to the stable operation of the system.

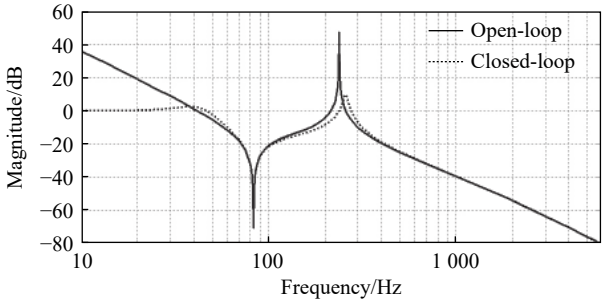

Fig. 4 Bode plots of the original system

The vibration caused by imaginary conjugate poles belongs to free vibration. In other words, if anti-resonance occurs, the motor speed keeps stable, and load speed oscillates, which has a trend of attenuation. It will not be excited by external disturbances. The vibration caused by imaginary conjugate zeros belongs to self-excited vibration. If control frequency equals the resonance frequency, the system will oscillate sharply and will not show a convergence trend.

Because of the inherent flexibility of the joint, the vibration caused by anti-resonance frequency appears as the residual vibration of the system. The vibration caused by resonance frequency appears as the resonance phenomenon excited by control frequency.

The time domain response and the frequency domain response of the system at the resonant frequency are obtained, as shown in Fig. 5 and Fig. 6. Fig. 5 illustrates the motor speed response of the closed-loop system at the resonant frequency. It can be observed that the amplitude seriously exceeds the given amplitude and the motor speed oscillates. The motor speed appears serious overshoot and the speed response appears high frequency oscillation in Fig. 6.

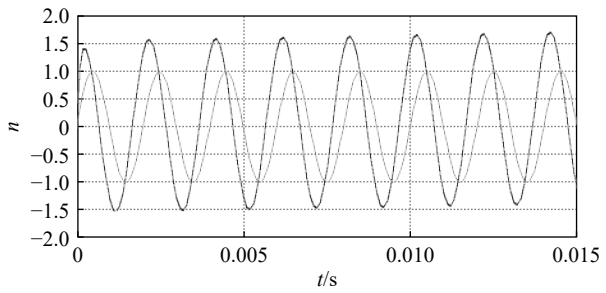

Fig. 5 Unit sinusoidal response of closed-loop system

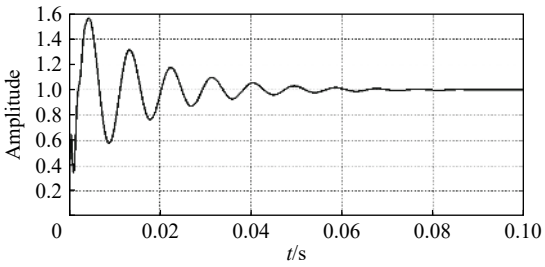

Fig. 6 Step response of motor speed

Based on the analysis mentioned above, if control frequency equals to the resonance frequency of the humanoid robot arm, the resonance will occur. Due to the coupling relationship between arm and motor, when the arm resonates, on the one hand, the speed and torque oscillate in the mechanical system. On the other hand, the output current and voltage amplitude fluctuate in the electrical control system. In the following, a PR controller is designed to deal with the above problem.

2 Resonance Suppression of Humanoid Robot Arm

2.1 PR controller

The humanoid robot arm resonates mainly at the specific frequency. If the control system frequency reaches the frequency at the resonance frequency, the arm will resonate. In order to suppress the resonant phenomenon and improve system stability, a PR controller is introduced to the humanoid robot control system.

The current controller $G_C(s)$ implemented in a synchronous frame rotating at frequency ω_0 is equivalent to the stationary frame controller[16]

$$G_{AC}(s) = G_{DC}(s - j\omega_0) + G_{DC}(s - j\omega_0) \quad (11)$$

where $G_{AC}(s)$ and $G_{DC}(s)$ represent the transfer functions of the current controller in the α-β coordinate system and the d-q coordinate system, respectively. If $G_C(s)$ is a PI controller, the corresponding transfer function in the α-β coordinate system is

$$G_{DC}(s) = G_{PI}(s) = K_p + \frac{K_i}{s} \quad (12)$$

where K_p and K_i are the proportional and the integrator coefficients, respectively. Take Eq. (12) into Eq. (11), we have

$$G_{AC}(s) = K_p + \frac{K_i s}{s^2 + \omega_0^2} \quad (13)$$

The transfer function of the PR controller in the α-β coordinate system is described in Eq. (13). Its Bode plot is shown in Fig. 7. It can be observed that the gain of the open-loop transfer function goes to infinity at s=jω_0 which can guarantee the zero-tracking-error for sinusoidal reference. However, the bandwidth of the controller is too narrow. To avoid stability problems associated with an infinite gain, the following can be used instead of Eq. (13) to give a non-ideal PR controller

$$G_c(s) = K_p + \frac{2K_i\omega_c(s + \omega_c)}{s^2 + 2\omega_c s + \omega_c^2 + \omega_0^2} \quad (14)$$

where K_r is the resonant coefficient, ω_c is the cutoff frequency. The bandwidth of the PR controller can be widened by setting ω_c appropriately, which can help reduce sensitivity towards slight frequency variation. Considering $\omega_c \ll \omega_0$, Eq. (14) can be simplified to

$$G_c(s) = K_p + \frac{2K_i\omega_c s}{s^2 + 2\omega_c s + \omega_0^2} \quad (15)$$

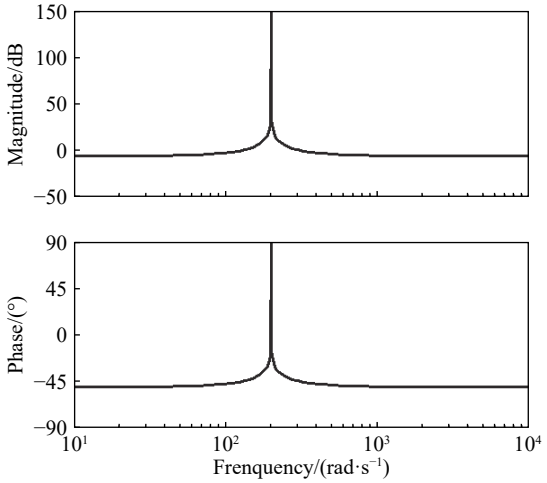

Fig. 7 Bode plot of open-loop PR current control system

Fig. 8 shows the frequency response waveforms of a PR controller when the cutoff frequencies are 5 rad/s, 10 rad/s, and 15 rad/s, respectively. The gain at the given resonant frequency

changes from infinite to a finite value $K_p + K_r$. Compared with the ideal PR controller, the cutoff frequency ω_c can be set appropriately to expand the controller bandwidth so as to decrease the sensitivity to the signal frequency variation, which improves the stability of control system. In practice, ω_c with the value of 5–15 rad/s is appropriate to ensure a suitable bandwidth[17].

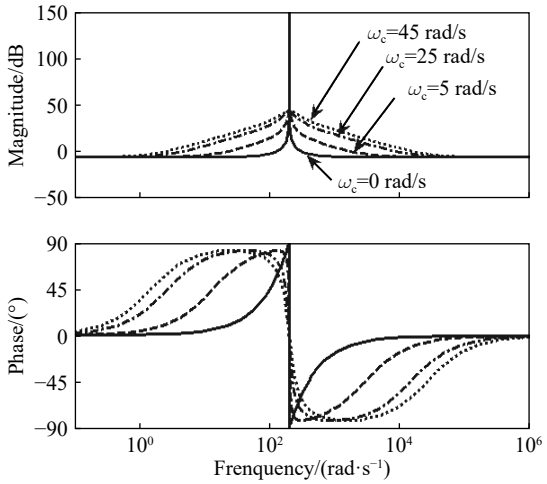

Fig. 8 Bode plot of open-loop PR current control system with different ω_c

2.2 Resonance suppression for humanoid robot arm based on PR controller

In the driving control system of humanoid robot, the control strategy of drive system for humanoid robot arm joint is designed based on the dynamic model of robot arm. The structural diagram of resonance suppression for humanoid robot arm based on the PR controller is shown in Fig. 9.

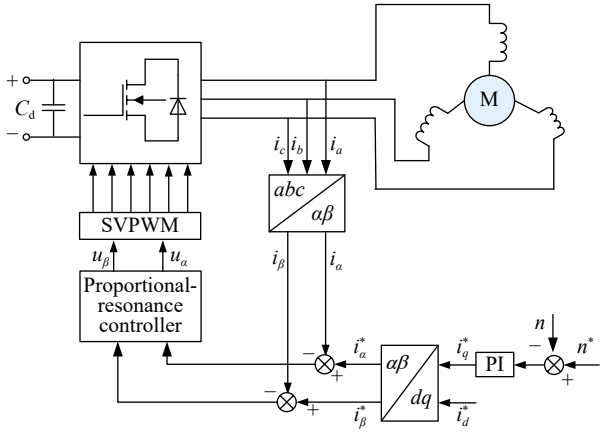

Fig. 9 Structural diagram of resonance suppression for humanoid robot arm

When control frequency equals the resonant frequency of arm, the resonance phenomenon occurs. According to the dynamical equation of the humanoid robot arm, there is a coupling relationship between the motion state of the arm and motor. The driving motor voltage will fluctuate when the motion state of the arm changes, which lead to output fluctuations of the controller under the circumstance of given input current. In the robot arm controller, the voltage fluctuation is given as a disturbance of the current closed loop.

The current-disturbance ratio rejection capability at null reference, for the control structure, demonstrated in Fig. 10, is defined as

$$F(s) = \frac{i(s)}{u_d(s)} = \frac{K_{PWM}G_{inv}(s)G_p(s)}{1 + K_{PWM}G_c(s)G_{inv}(s)G_p(s)} \quad (16)$$

where i is the actual AC input current, u_d is considered as the disturbance for the system, K_{PWM} is the equivalency gain of the inverter. And the transfer function of the inverter is given by

$$G_{inv}(s) = \frac{1}{T_s s + 1} \quad (17)$$

where T_s is the switching time. Because of high switching frequency, it is generally ignored by the processing delay and sample delay for analysis. The inverter unit is approximated as a proportional link with small inertia.

The transfer function of the robot arm joint motor is defined as

$$G_p(s) = \frac{1}{Ls + R} \quad (18)$$

where L and R are equivalent inductance and resistance, respectively. Since Eq. (18) is first-order inertia, its time constant is $T_p = L/R$.

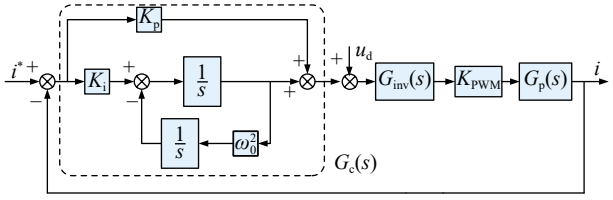

Fig. 10 Block diagram of the current loop based on PR controller

The Bode plot of disturbance rejection for a PR controller is shown in Fig. 11. As it can be observed, around the resonance frequency the PR controller provides a large attenuation of amplitude. Besides, it is clear that PR has the characteristic of rejection capability at a specific frequency from Fig. 8.

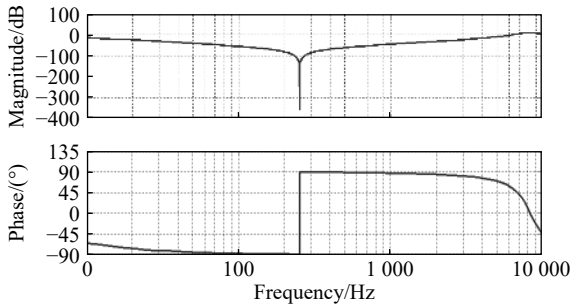

Fig. 11 Bode plot of disturbance rejection of a PR controller

The frequency of the output of the control signal is the same as the voltage disturbance signal when the current reference is constant. If the frequency of output signal equals the arm resonance frequency, the self-excited oscillation will occur. Furthermore, the resonance phenomenon occurs. The PR controller uses the ideal expression shown in Eq. (13) and its frequency ω_0 is set to the arm resonant frequency ω_{NTF}.

$$F(s)\,|_{s=\mathrm{j}\omega_{\mathrm{NTF}}} = \frac{K_{\mathrm{PWM}}G_{\mathrm{inv}}(s)G_{\mathrm{p}}(s)}{1+K_{\mathrm{PWM}}G_{\mathrm{c}}(s)G_{\mathrm{inv}}(s)}\,|_{s=\mathrm{j}\omega_{\mathrm{NTF}}} = 0 \tag{19}$$

Eq. (19) shows that the PR controller has the rejection capability to the voltage disturbance at the resonant frequency. After the PR controller is introduced, the output current of inverter is not affected by vibration at the resonant frequency. Hence, the self-excited oscillation of the system is avoided when the frequency of the inverter output signal is equal to the arm resonance frequency.

The PR controller parameters are designed with the basis on the root-locus method to suppress the disturbance signal. The open-loop transfer function of the current loop shown in Fig. 10 is represented as

$$H(s) = K_{\mathrm{PWM}}G_{\mathrm{c}}(s)G_{\mathrm{p}}(s) = K_{\mathrm{PWM}}\frac{K_{\mathrm{p}}s^2+K_{\mathrm{i}}s+K_{\mathrm{p}}{\omega_0}^2}{(s^2+{\omega_0}^2)(Ls+R)} \tag{20}$$

where $K_{\mathrm{s}} = K_{\mathrm{PWM}}K_{\mathrm{p}}$ is set to be the open-loop equivalent gain of the current loop and $\tau_{\mathrm{i}} = K_{\mathrm{p}}/K_{\mathrm{i}}$ is the equivalent time constant of the PR controller. Thus, Eq. (20) can be rewritten as

$$H(s) = \frac{K_{\mathrm{s}}(s^2+\frac{1}{\tau_{\mathrm{i}}}s+{\omega_0}^2)}{(s^2+{\omega_0}^2)(Ls+R)} \tag{21}$$

The root-locus of the current closed-loop is represented in Fig. 12 when the equivalent gain K_{s} increases from zero to infinity. The equivalent time constant τ_{i} of four curves is 3 ms, 5 ms, 7 ms, and 9 ms, respectively. Based on the pole-zero cancellation method, the current controller can be set efficiently. Normally, the equivalent time constant τ_{i} is set as $\tau_{\mathrm{i}} = T_{\mathrm{p}}$[18].

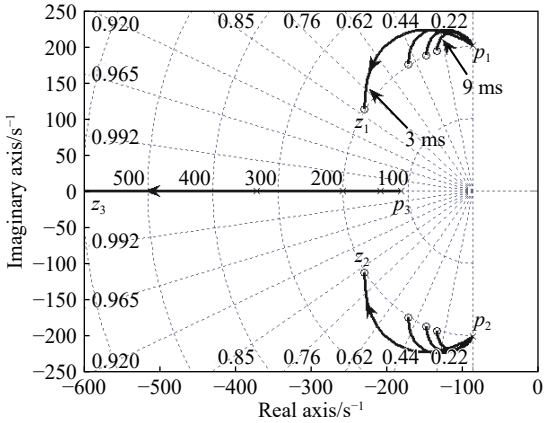

Fig. 12 Root-locus of the current controller

Fig. 12 illustrates the eigenvalue of the control system distribute in left semi-plane on s domain under different time constants. When the damping ratio of the control system is between 0.4 and 0.8, the system overshoot is small, and the speed response is fast. The expected damping performance can be obtained through the root-locus method. The range of the proportional coefficient is $K_{\mathrm{p}} \in [0.11, 0.75]$, and the range of the resonant coefficient is $K_{\mathrm{r}} \in [37, 250]$.

A PR controller is introduced to the humanoid robot arm system and its the block diagram is shown in Fig. 13. Fig. 14 shows the Bode plot of the open-loop and closed-loop system of robot arm with the PR controller. The gain of open-loop system attenuates to 0.203 dB at the resonant frequency. The PR controller adds

damping to the system and increases gain margins of the system. It is observed that the gain of the open-loop resonance frequency of the system can be effectively attenuated after the PR controller is added to the current loop. Additionally, the step response of the system using the PR controller is shown in Fig. 15. It can be seen that the oscillation is eliminated and the response speed increases. The system stability is improved.

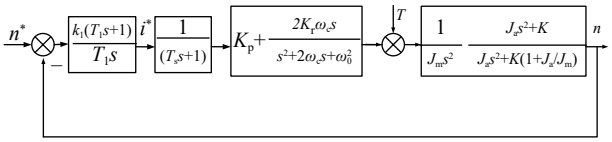

Fig. 13 Block diagram of humanoid robot arm with PR controller

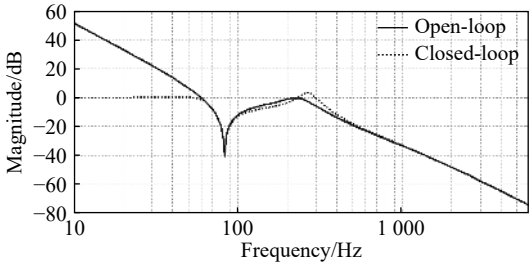

Fig. 14 Bode plot of open-loop and closed-loop system with PR controller

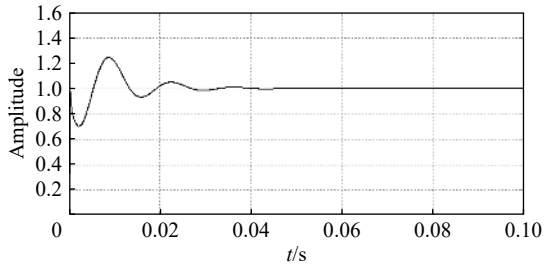

Fig. 15 Step response of motor speed with PR controller

3 Simulation and Analysis

In order to verify the effectiveness of the resonance suppression scheme for the humanoid robot arm based on PR controller, this paper uses MATLAB/Simulink to build a model for simulation verification.

The parameters of the BLDC motor are as follows: pole pairs p=4, the rated voltage is 12 V, the armature resistance R is 24 Ω, the rated torque is 0.5 N·m, the rated speed is 1000 r/min, the equivalent inductance is 1.4 mH, and the rotational inertia coefficient is 0.000 62 kg·m^2. The moment of inertia of the humanoid robot arm is 0.004 5 kg·m^2, and the link length is 0.15 m. The joint stiffness coefficient is 10.

In the simulation process, the BLDC motor starts with no load. The given speed of the motor is set to 1 000 r/min, the current PR controller parameters are set as to $k_p = 0.5$, $k_r = 150$, $\omega_c = 10$ rad/s. The control effect of the resonance suppression strategy for the humanoid robot arm joint based on the PR controller is observed in simulation. Fig. 16 shows the joint motor simulation results for humanoid robot arm under the disturbance. Fig. 16a is the current waveforms, and the speed and torque curves are shown in Fig. 16b and Fig. 16c, respectively.

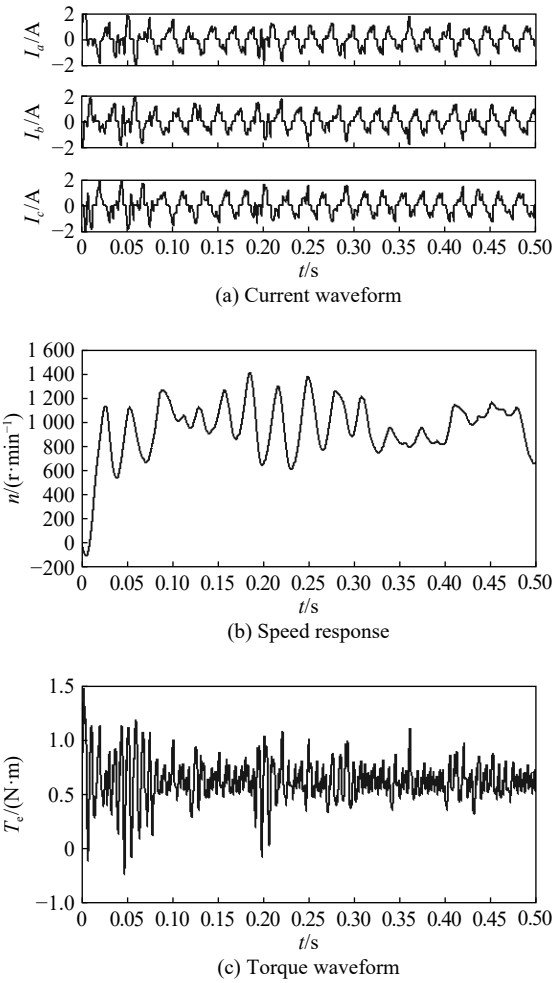

Fig. 16 Simulation waveforms without PR controller

The disturbance signal with the frequency equals resonance frequency is added in simulation. The results imply that the voltage disturbance causes an additional and unexpected current, resulting in current distortion in three-phases. Besides, it is observed that the rotational speed and torque oscillates.

Simulation results of phase current, speed and torque waveforms when utilizing the PR controller are illustrated in Fig. 17. As shown in Fig. 17a, when the resonance occurs, under the control of the proposed PR controller, the current waveforms are close to an ideal trapezoidal form at 0.15 s. The current distortion is reduced. Fig. 17b shows the A-phase current waveforms. After 0.15 s, the motor output torque remains stable with a little fluctuation. At 0.15 s, the speed reaches 1000 r/min, which is within the allowable error range. And then the speed keeps stable.

Compared with the simulation waveforms under voltage disturbance without the PR controller, it can be seen that PR controller has the good effect of disturbance rejection at the specific frequency. When the disturbance is suppressed, the phase current maintains rectangular waveforms, the speed curve is stable, and the torque has little fluctuations. It is obvious that the resonance suppression for humanoid robot arm based on PR controller is effective. As a result, the dynamic performance and system stability are improved.

Compared with the simulation waveforms under voltage disturbance without the PR controller, it can be seen that PR controller has the good effect of disturbance rejection at the specific frequency. When the disturbance is suppressed, the phase current maintains rectangular waveforms, the speed curve is stable, and the torque has little fluctuations. It is obvious that the resonance suppression for humanoid robot arm based on the PR controller can effectively suppress the resonance phenomenon. As a result, the dynamic performance and system stability are improved.

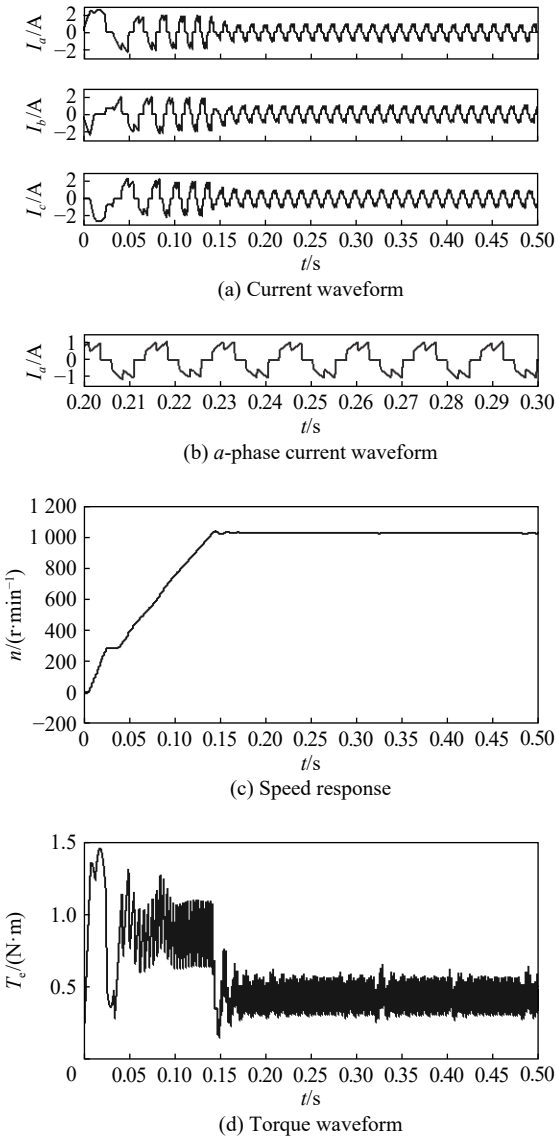

Fig. 17 Simulation waveforms based on PR controller

4 Conclusion

This paper presents a resonance suppression strategy for a humanoid robot arm based on a PR controller, which solves the problem caused by the control frequency and resonance frequency, since the driving motor voltage will fluctuate when the motion state of the arm changes. The fluctuation is regarded as the disturbance of closed-loop current control. The PR controller has the characteristic of disturbance rejection at the specific frequency without affecting the performance at other frequencies. The output current of the inverter will not be affected by the vibration of the arm at the resonance frequency.

Consequently, the control frequency will not equal to the arm resonant frequency so that the self-excited oscillation will not be excited. The simulation results show that the proposed strategy has a good resonance suppression effect at a specific frequency. The total system has a very simple structure and the resonance of humanoid robot arm was well suppressed by the proposed method. The new strategy also improves the stability of the system, ensuring that the system has a good dynamic performance.

References:

[1] Benosman M, Le Vey G. Control of flexible manipulators: A survey [J]. Robotica, 2004, 22(5): 533-545.

[2] Pereira E, Aphale S S, Feliu V, et al. Integral resonant control for vibration damping and precise tip-positioning of a single-link flexible manipulator [J]. IEEE/ASME Transactions on Mechatronics, 2011, 16(2): 232-240.

[3] Rong Jili, Xiang Yang, Xin Pengfei, et al. Vibration control and experiment research of two-link flexible manipulator considering flexibility of the joint[J]. Journal of Astronautics, 2017, 38(10): 1024-1031. (in Chinese)

[4] Yang Ming, Hu Hao, Xu Dianguo. Cause and suppression of mechanical resonance in PMSM servo system [J]. Electric Machines & Control, 2012, 16(1): 79-84. (in Chinese)

[5] Kumagai S, Ohishi K, Miyazaki T. High performance robot motion control based on zero phase error notch filter and D-PD control[C]// IEEE International Conference on Mechatronics, IEEE, 2009.

[6] Yang Ming, Hao Liang, Xu Dianguo. Online suppression of mechanical resonance based on adapting notch filter [J]. Journal of Harbin Institute of Technology, 2014, 46(4): 63-69. (in Chinese)

[7] Kang C I, Kim C H. An adaptive notch filter for suppressing mechanical resonance in high track density disk drives [J]. Microsystem Technologies, 2005, 11(8-10): 638-652.

[8] Hori Y, Sawada H. Slow resonance ratio control for vibration suppression and disturbance rejection in torsional system [J]. IEEE Transactions on Industrial Electronics, 1999, 46(1): 162-168.

[9] Seki Y, Fujimoto H, Saiki K. Optimal mechanical parameter design using self resonance cancellation control for gantry-type high precision stage[C]// IEEE International Workshop on Advanced Motion Control, IEEE, 2012.

[10] Motonobu Aoki, Hiroshi Fujimoto, Yoichi Hori, et al. Robust resonance suppression control based on self resonance cancellation disturbance observer and application to humanoid robot[C]// IEEE International Conference on Mechatronics, IEEE, 2013.

[11] Citro C, Siano P, Cetati C, et al. Designing inverters' current controllers with resonance frequencies cancellation [J]. IEEE Transactions on Industrial Electronics, 2016, 63(5): 3072-3080.

[12] Fantino R, Busada C, Solsona J. Optimum PR control applied to LCL filters with low resonance frequency [J]. IEEE Transactions on Power Electronics, 2017, 33(1): 793-801.

[13] Kamyar S, Mehrdad M. An adaptive PR Controller for synchronizing grid-connected inverters [J]. IEEE Transactions on Industrial Electronics, 2018, 66(3): 2034-2043.

[14] Spong M W. Modeling and control of elastic joint robots [J]. Journal of Dynamics Systems Measurement and Control, 1987, 109(4): 310-319.

[15] Mario Ramirez-Neria, Gilberto Ochoa-Ortega, Norma Lozada-Castillo, et al. On the robust trajectory tracking task for flexible-joint robotic arm with unmodeled dynamics [J]. IEEE Access, 2016, 4: 7816-7827.

[16] Teodorescu R, Blaabjerg F, Liserre M, et al. Proportional-resonant controllers and filters for grid-connected voltage-source converters [J]. IEE Proceedings-Electric Power Applications, 2006, 153(5): 750.

[17] Liu Bin, Wu Jiaju, Li Jun, et al. A novel PFC controller and selective harmonics suppression [J]. International Journal of Electrical Power & Energy Systems, 2013, 44(1): 680-687.

[18] Lascu C, Asiminoaei L, Boldea I, et al. High performance current controller for selective harmonic compensation in active power filters [J]. IEEE Transactions on Power Electronics, 2007, 22(5): 1826-1835.